Environ. Sci. Technol. **2005**, *39,* 188−194

Speciation of Iron and Sulfate in Acid Waters: Aqueous Clusters to Mineral Precipitates

JURAJ MAJZLAN*,† AND SATISH C. B. MYNENI†,‡

Department of Geosciences, Princeton University, Princeton, New Jersey 08544, and Earth Sciences Division, Lawrence Berkeley National Laboratory, Berkeley, California 94720

Acid mine drainage (AMD) contaminates surface water bodies, groundwater, soils, and sediments at innumerable locations around the world. AMD usually originates by weathering of pyrite (FeS_2) and is rich in Fe and sulfate. In this study, we investigated speciation of Fe^{II}, Fe^{III}, and SO_4 in acid waters by Fourier transform infrared and X-ray absorption spectroscopy. The molalities of sulfate (15 mmol/kg) and iron (10, 20, and 50 mmol/kg), and pH (1, 2, and 3) were chosen to mimic the concentration of ions in AMD waters. Sulfate and Fe^{II} either associate in outer-sphere complexes or do not associate at all. In contrast, sulfate interacts strongly with Fe^{III}. The predominating species in $Fe^{III}-SO_4$ solutions are hydrogen-bonded complexes; inner-sphere complexes account only for 10 ± 10% of the total sulfate. Our results show that the mode of interaction between Fe^{III} and sulfate is similar in aqueous phase and in nanocrystalline precipitate schwertmannite ($\sim FeO(OH)_{3/4}(SO_4)_{1/8}$). Because of this similarity, schwertmannite should be the phase that controls solubility and availability of Fe^{III}, SO_4, and indirectly also other components in the AMD solutions.

Introduction

Acidic water input from atmospheric deposition (*1*, *2*) and pyrite weathering (*3*, *4*) is a growing global environmental problem that threatens to alter soil geochemistry significantly. Sulfate is a predominant ion in these waters, and its interaction with monomeric and polymeric forms of iron and aluminum plays a central role in the solubility, speciation, and toxicity of these and other associated ions. The equilibrium constants that are widely used to describe the behavior of these aqueous ions (*5*) predict a strong tendency of trivalent cations and sulfate to associate in such solutions to form complexes. However, the exact nature of these complexes remains unknown.

Among the major components of acid waters, the system $Fe^{III}-SO_4$ receives special attention because of its frequent occurrence and its influence on the solubility and mobility of trace elements in the acid solutions (*6*). Previous thermodynamic studies of the $Fe^{III}-SO_4$ solutions predicted free sulfate, hydrogen sulfate, complexes $[Fe(SO_4)_n]^{3-2n}$, $[Fe(HSO_4)]^{2+}$, and iron oligomers (*7*−*9*), whose existence is either assumed or discerned by fitting the results of bulk measurements. Most of these investigations consider interactions between monomeric Fe^{III} and sulfate. Only a few studies take dimers (*8*) and polymers into account, although their existence has been suggested by spectroscopic data (e.g., ref *10*). None of these studies derives association constants for the Fe^{III} polymers and sulfate. The neglect of such an interaction is surprising given that the constants for monomeric species imply strong association of Fe^{III} monomers and sulfate.

Supporting molecular information for the existence and structure of the aqueous species does not enter the thermodynamic calculations, which leaves a gap in the understanding of Fe−sulfate speciation and its influence on trace metal solubility and transport in polluted acid systems. Hence, the goal of this study is to provide the molecular information for the aqueous systems $Fe^{II}-SO_4$ and $Fe^{III}-SO_4$. These two systems were chosen because their components are the major constituents in acid mine drainage (AMD) discharges that are the product of pyrite weathering at innumerable locations around the world (*11*). AMD waters are often oxidized, with Fe^{III} being more abundant than Fe^{II}. Therefore, we place greater emphasis on the aqueous systems with Fe^{III} and SO_4 as the dominant components.

Speciation of acidic solutions rich in iron and sulfate was determined using infrared and X-ray absorption spectroscopic techniques. We then proceeded to link the structure of aqueous ions with the structure of nanocrystalline precipitates that frequently form from AMD waters.

Experimental Section

Sample Preparation. Solutions examined in this investigation were prepared using deionized water and reagent grade Na_2SO_4, $FeCl_2{\cdot}4H_2O$, $FeCl_3{\cdot}6H_2O$, and $Fe(NO_3)_3{\cdot}9H_2O$. Metal solutions of 40, 80, and 200 mmol/kg were prepared by mixing deionized water and a metal salt. Deionized water was acidified with 37% HCl or 60% HNO_3 close to the desired pH. The acid used was matching the anion of the Fe salts (i.e., the solutions contained either chloride or nitrate, but never both these anions). An appropriate amount of the acidified water was mixed with Na_2SO_4 to prepare 20 mmol/kg SO_4 solution. The metal solutions were then diluted either by acidified water or by acidified Na_2SO_4 solution to achieve final molalities of 15 mmol/kg for SO_4 and 10, 20, or 50 mmol/kg for the metal. The pH was then adjusted to the desired value (1, 2, or 3; ± 0.1) with the required amount of HCl or HNO_3. Sample pH was measured with a glass electrode calibrated with pH 7.00 and pH 4.01 buffers. The samples were kept at room temperature throughout preparation and spectra collection.

The exact concentration of all components in our solutions is not known. The molalities of sulfate, iron, and sodium are fixed by the amounts of Na_2SO_4 and Fe salts added. The concentration of Cl^- or NO_3^- is not precisely known because variable amounts of either HCl or HNO_3 were added to adjust pH. Therefore, we do not know the ionic strength of these solutions. However, even knowing the concentration of all components, only stoichiometric ionic strength could be calculated; the real ionic strength, strongly influenced by ion pairing, is significantly different.

Infrared Spectroscopy. Infrared spectra were collected in attenuated total reflectance (ATR) mode, using a Bruker IFS 66 v/s Fourier transform infrared (FTIR) spectrometer. Solutions were held in a 12 reflection horizontal 45° AMTIR-ATR accessory, and the signal was detected by a liquid nitrogen cooled MCT detector. Background spectra in all

* Corresponding author present address: Institute of Mineralogy, Petrology and Geochemistry, Albert-Ludwig-University of Freiburg, Albertstrasse 23b, Freiburg D-79104, Germany; phone: +49-761-203-6416; fax: +49-761-203-6407; e-mail: Juraj.Majzlan@minpet.uni-freiburg.de.

† Princeton University.

‡ Lawrence Berkeley National Laboratory.

10.1021/es049664p CCC: $30.25
Published on Web 11/18/2004

cases were determined using deionized water. The spectra presented here are the difference between the spectra of metal−sulfate solution and those of metal solution of equal metal molality and pH. The infrared spectra were collected within 10 min from preparation of the solution in order to minimize effects of oxidation of Fe^{II}, polymerization, and precipitation. An aging experiment, in which spectra of Fe^{III}−SO_4 solutions were collected daily for several days, is described separately. Peak fitting was done with GRAMS/AI (Thermo Galactic) software. The FTIR peaks were modeled by a pseudo-voigt function in GRAMS/AI; the refined parameters included peak position, height, width, and fraction of the Lorentzian component.

The FTIR spectra of solids were collected in ATR mode with the same spectrometer. The solids were pressed on a single reflection diamond-ATR accessory, and the signal was detected by a DTGS detector.

X-ray Absorption Spectroscopy. The X-ray absorption near-edge structure (XANES) spectra at sulfur K edge were collected at the Stanford Synchrotron Radiation Laboratory (Menlo Park, CA) using beamline 6-2 and a Si (111) monochromator. A He flight path chamber was used to enhance incident photon flux. Higher order X-rays were rejected using Ni-coated mirrors. The X-ray absorption spectra were collected in fluorescence mode using a Lytle-type detector. Some of the samples were also examined at the National Synchrotron Light Source (Upton, NY), beamline X-19A, using a similar setup. The monochromator at this beamline was detuned by 50% at the S-absorption edge to reduce the higher order harmonics. Step size of 0.5 eV was used in the energy regions 2460.0−2468.5 and 2500.0−2549.5 eV, and step size of 0.08 eV was used between 2468.5 and 2500.0 eV. Integration time of 1−2 s was used at each step. All of the sulfate spectra were calibrated against the low-energy transition in solid $Na_2(SO_3S)\cdot 5H_2O$, which was set at 2469.2 eV. The spectra of $Na_2(SO_3S)\cdot 5H_2O$ were collected frequently during the XANES data measurements to correct for the systematic error associated with the drift of the monochromator. The X-ray absorption spectra were averaged and normalized with the WINXAS software (*12*). The preedge region of the solution spectra was fit by a set of reference spectra using the linear combination utility of WINXAS. Linear least-squares fit of a sample spectrum using a combination of reference spectra is commonly used for interpretation of XANES spectra (e.g., ref *13*).

X-ray Diffraction (XRD). XRD patterns of the solids used in this study were collected with a Scintag PAD V diffractometer, employing Cu Kα radiation, diffracted beam graphite monochromator, and a scintillation detector. The identity and purity of the solids was verified by Rietveld refinement, using GSAS (*14*).

Results

To monitor the speciation of Fe−SO_4 solutions, we focused on detection and interpretation of infrared and X-ray spectral features that indicate modification of sulfate anion by protonation, metal complexation, or hydration. While the infrared spectra are sensitive to all these coordination environments, the X-ray absorption spectra of sulfur are sensitive specifically to the protonation and Fe complexation of sulfate. Fe^{III}−SO_4 solutions were investigated by both spectroscopic techniques; Fe^{II}−SO_4 solutions were investigated only by FTIR spectroscopy. The molalities of sulfate (15 mmol/kg) and iron (10, 20, and 50 mmol/kg) and pH (1, 2, and 3) were chosen to mimic the concentration of ions in AMD waters.

Infrared Spectroscopy. The variations in symmetry of the sulfate anion, number of infrared active bands, and their approximate energies were discussed in detail by Hug (*15*). Here we only summarize this information to aid in interpretation of our FTIR spectra. The infrared spectrum of

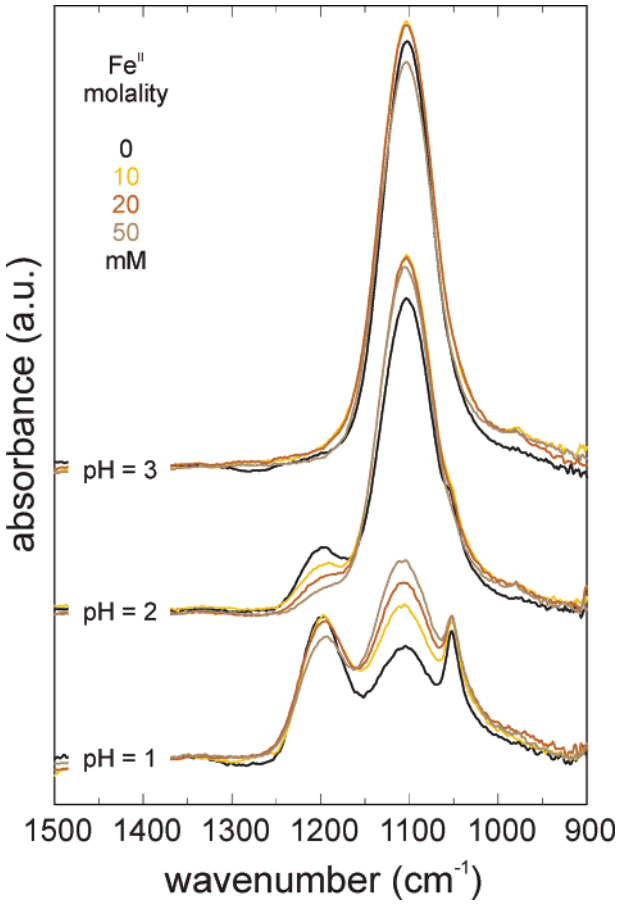

FIGURE 1. Infrared spectra of Fe^{II}−SO_4 solutions at pH 1, 2, and 3; $\sum SO_4$ = 15 mmol/kg; and variable Fe^{II} molality.

undistorted sulfate in aqueous solutions of Na_2SO_4 shows an asymmetric SO_4 stretching band at 1102 cm^{-1} (Figure 1). Distortion of sulfate by protonation (i.e., formation of hydrogen sulfate) leads to the appearance of asymmetric and symmetric SO_3 stretching bands at 1200 and 1050 cm^{-1}, respectively (Figure 1), and an S−OH stretching band at 890 cm^{-1} (*15*).

Changes in the intensities of the sulfate and hydrogen sulfate bands are dictated by the sulfate/hydrogen sulfate ratio in the solution. This ratio is controlled by both pH (Figure 1) and ionic strength (Figure 2) of the solution. At infinite dilution, sulfate and hydrogen sulfate occur at equal concentration at pH = pK_a = 1.96 (*16*), and hydrogen sulfate predominates at lower pH. Sulfate is also favored by increasing ionic strength of the solution (*16*) (Figure 2).

Distortion of sulfate by hydrogen bonding and Fe^{III} complexation (*15*, *17*, *18*) will also result in changes of symmetric and asymmetric stretching vibration, but their energies are different from those of hydrogen sulfate. To identify the coordination environment of Fe^{III}−sulfate complexes, we examined FTIR spectra of numerous iron−sulfate minerals jarosite (nominal composition $KFe_3(SO_4)_2(OH)_6$), copiapite ($Fe^{2+}Fe^{3+}{}_4(SO_4)_6(OH)_2\cdot 20H_2O$), rhomboclase ($(H_5O_2)$-$Fe(SO_4)_2\cdot 3H_2O$), roemerite ($Fe^{2+}Fe^{3+}{}_2(SO_4)_4\cdot 14H_2O$), and synthetic ferric ammonium alum ($NH_4Fe(SO_4)_2\cdot 12H_2O$). These phases exhibit different types of sulfate linkages with Fe^{III} octahedra, either direct coordination or hydrogen-bonding interaction. The spectra of ferric sulfate solids show a well-separated S−O−Fe or S−O···H stretching band at 980−1010 cm^{-1}. The remaining asymmetric and symmetric vibrations of the sulfate ion usually overlap in a broad band centered near 1100 cm^{-1}. Similarly, sulfate in Fe^{III} solutions or on surfaces of iron oxides shows a distinct S−O−Fe or S−O···H

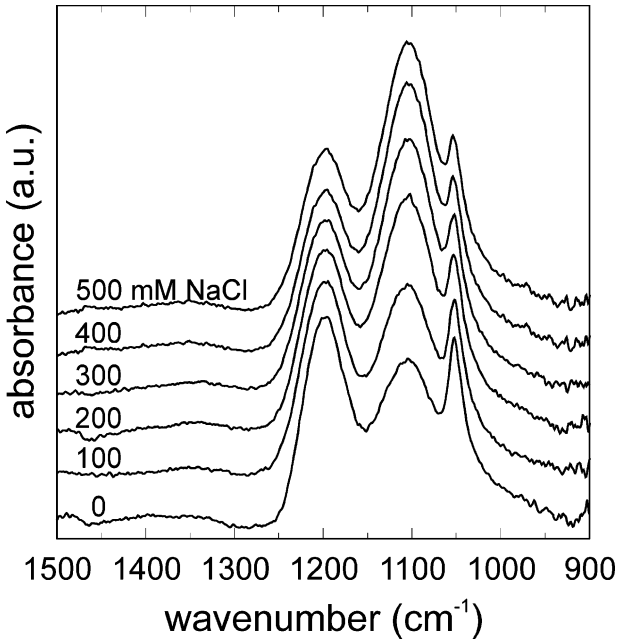

FIGURE 2. Infrared spectra of Na_2SO_4 solution as a function of ionic strength. pH 1, $\sum SO_4$ = 15 mM. The spectra document the effect of ionic strength on the sulfate/hydrogen sulfate ratio in the solutions.

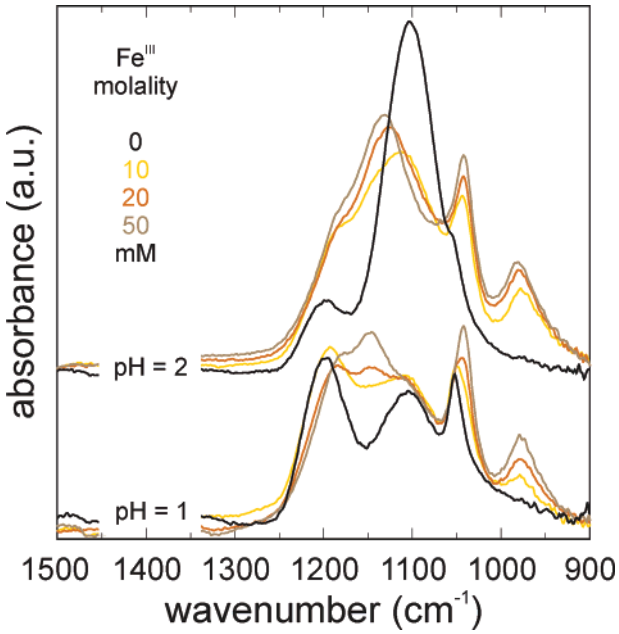

FIGURE 3. Infrared spectra of Fe^{III}–SO_4 solutions at pH 1 and 2, $\sum SO_4$ = 15 mmol/kg, and variable Fe^{III} molality.

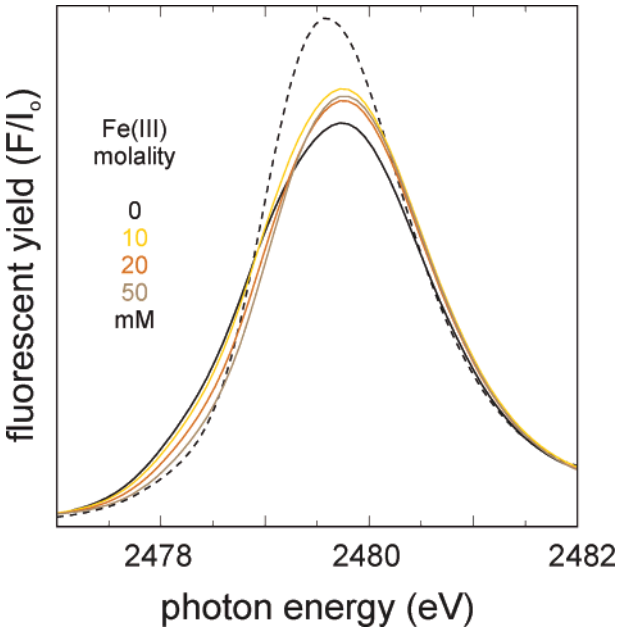

FIGURE 4. X-ray absorption spectra of Fe^{III}–SO_4 solutions at pH 1 (colored solid curves) and Na_2SO_4 solution at pH 1 (black solid curve) and at pH 6 (black dashed curve).

stretching band at 950–980 cm^{-1} and a series of overlapping bands at 1020–1270 cm^{-1} (*15*). Therefore, sulfate ion distorted by iron complexation or hydrogen bonding is distinguished from hydrogen sulfate by the stretching band at 950–980 cm^{-1} versus 890 cm^{-1}, respectively.

Addition of Fe^{II} to the sulfate solution caused only minor changes in the FTIR spectra (Figure 1). Peak position remained the same as for the solutions with no Fe^{II}. A very weak band at 980 cm^{-1} can be seen in the spectra collected at pH 2 and 3. The variation in the intensity of the observed bands (Figure 1) can be explained by the ionic strength effect on the sulfate/hydrogen sulfate ratio in the solutions.

When Fe^{III} was added to the sulfate solutions at pH 1 and 2, the infrared spectral contributions of sulfate and hydrogen sulfate diminished and new bands appeared between 950 and 1250 cm^{-1} (Figure 3). There may be several new bands in the spectral region between 1100 and 1150 cm^{-1}. Of these, the band at 1150 cm^{-1} can be well resolved only in the spectra of pH 1 solutions (Figure 3). The intensity of the band increases with increasing Fe^{III} molality. The overlap of the new bands and the sulfate band at 1102 cm^{-1} causes shift of the spectral feature that dominates the spectra in the 1100–1150 cm^{-1} region. The hydrogen sulfate band at 1050 cm^{-1} overlaps with a strong band at 1042 cm^{-1}; the latter band is present only when Fe^{III} is present in the solution. The high-energy shoulder is located at 1194 cm^{-1}, and at pH 1 overlaps with the hydrogen sulfate band at 1200 cm^{-1}. A distinct new band appeared at 976 cm^{-1} (Figure 3). Experiments at higher pH values could not be performed with Fe^{III} because of rapid precipitation at pH ≥ 2.5.

The speciation of Fe^{III} and sulfate was investigated in solutions prepared from both chloride and nitrate of Fe^{III}. No differences were observed among the FTIR spectra of these two sets of solutions, indicating that neither chloride nor nitrate interfere strongly with the iron(III)–sulfate complexes.

Aging of the Fe^{III}–SO_4 solutions was monitored by FTIR spectroscopy for 7 consecutive days. Four solutions that were used in this experiment had $\sum SO_4$ molality of 15 mmol/kg, Fe^{III} molality of 10 or 50 mmol/kg, and pH 1 or 2. No differences were found among the positions or the widths of the spectral bands in comparison with spectra collected immediately after the solutions were prepared. The temporal invariability of the spectra suggests that the local coordination of sulfate is established rapidly and does not change as the solutions age.

X-ray Absorption Spectroscopy. The X-ray absorption spectrum of Na_2SO_4 solution at pH 6 shows a sharp absorption edge at 2479.6 eV (Figure 4), assigned to the transition of 1s–t_2^* orbitals in sulfur (*18*). With protonation of sulfate, the main absorption edge of sulfate broadens, and the peak maximum shifts to higher energy by ~0.4 eV. This spectral broadening is caused by changes in the symmetry of sulfate and associated splitting of the triply degenerate t_2^* orbitals.

Additional weak features appear ~2.0 eV below the S-absorption edge in the spectra of the studied solutions and ferric sulfate minerals. These preedge features are caused

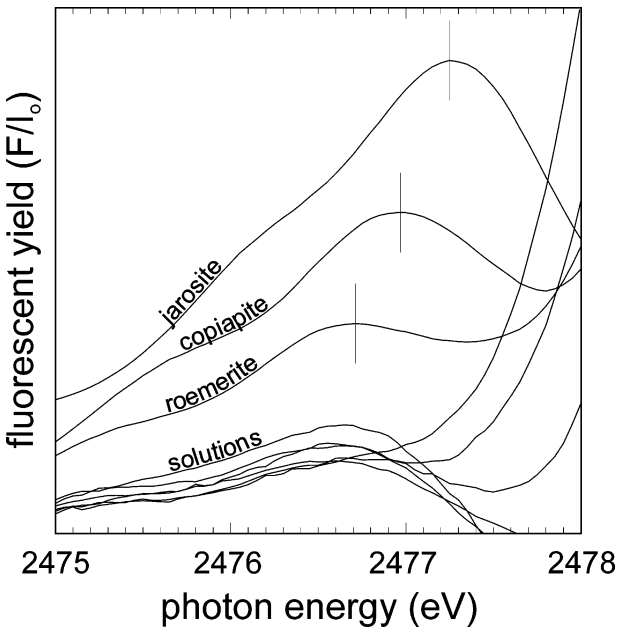

FIGURE 5. Preedge features in the X-ray spectra of the reference solids and $Fe^{III}-SO_4$ solutions at pH 1 and 2. To magnify the weak preedge features, the spectrum of aqueous sulfate was subtracted from the normalized sample spectra. The short vertical lines show the position. The spectra are offset for clarity.

by the 1s electronic transition from sulfur orbitals to hybridized iron 3d orbitals (*19*) and can arise only if the iron ion is directly bonded to sulfur via a bridging oxygen. In aqueous solution, such arrangement corresponds to an inner-sphere complex.

The energy of the preedge features is a sensitive indicator of the connectivity between iron and sulfur polyhedra (*20*). Sulfate shares one, two, or three oxygens with the adjacent iron octahedra, as in the crystal structures of roemerite, ferricopiapite, and jarosite, respectively. The shift of the preedge features to higher energy is concomitant with an increase in the number of oxygens shared among the sulfate and iron polyhedra. In roemerite, only one oxygen is shared between sulfur and iron, and the preedge feature occurs at 2476.8 eV (Figure 5). Increasing the number of shared oxygen to two or three in ferricopiapite and jarosite, respectively, leads to shift of the preedge feature to 2477.0 and 2477.3 eV, respectively (Figure 5).

The X-ray spectra of the $Fe^{III}-SO_4$ solutions exhibit weak preedge features (Figure 5). A numerical estimate of the fraction of inner-sphere complexes in solutions was obtained by a linear combination of the preedge region of a reference solid spectrum and the spectrum of Na_2SO_4 solution. The concentration of inner-sphere complexes in *all studied Fe^{III} solutions* (pH 1 or 2; Fe^{III} = 10, 20, or 50 mmol/kg, ΣSO_4 = 15 mmol/kg) is 10% of total sulfate. The error on this estimate is dominated by uncertainties related to the normalization procedure and selection of the reference spectra for linear combination. The reproducibility of the spectra was excellent and contributed little to this error, even though the intensity of the preedge feature in solution spectra was only 1−2% of the intensity of the main edge. Therefore, the choice of low-energy region for normalization to 0, and the postedge jump for normalization to 1, was affecting the value of the estimate. The value of estimate changed slightly also with different choices of spectra of the reference solids. Choosing different regions for normalization and different reference spectra for the linear combination led to a scatter of 5 percentage points (i.e., to 10 ± 5% of inner-sphere complexes in the solutions). To better account for these variations, we consider a double error of 10 ± 10% a realistic value for the fraction of inner-sphere complexes.

The structural environment of the inner-sphere complex is identified by comparing the preedge energies of solutions with the examined reference solids. The energy of these preedge features indicates that monodentate inner-sphere complexes are much more abundant than the bi- or tridentate species (Figure 5). Because the measured signal is strongly dominated by the monodentate complexes, we are not able to distinguish the contribution of bidentate or tridentate complexes. In addition, we are not able to detect complexes of multiple sulfate tetrahedra bound to a single iron octahedron, such as $[Fe(SO_4)_2]^-$, analogous to the complexes $[Al(SO_4)_2]^-$ proposed in $Al^{III}-SO_4$ solutions (*21*). The techniques used in this study probe only the sulfate ion and cannot distinguish the complexes $[Fe(SO_4)_2]^-$ and $[Fe(SO_4)]^+$.

Discussion

Speciation of $Fe^{II}-SO_4$ Solutions. FTIR spectra of $Fe^{II}-SO_4$ solutions (Figure 1) indicate that the interaction of sulfate with Fe^{II} is negligible. Sulfate and Fe^{II} either associate in outer-sphere complexes or do not associate at all. The lack of inner-sphere interaction is a common feature to the aqueous solution and melanterite ($FeSO_4 \cdot 7H_2O$), the phase that would crystallize from more concentrated $Fe^{II}-SO_4$ solution at room temperature (*22*). In other words, speciation of the solution is reflected in the structure of the corresponding crystalline solid.

Speciation of $Fe^{III}-SO_4$ Solutions. The infrared spectral features indicate a significant distortion of sulfate ion when Fe^{III} is added to sulfate solutions at all examined pH values and Fe^{III} concentrations (Figure 3). Linear combination of the reference X-ray absorption spectra gave an estimate of 10 ± 10% of inner-sphere complexes in the $Fe^{III}-SO_4$ solutions. In contrast to the X-ray spectroscopy investigations, changes in the infrared spectra of $Fe^{III}-SO_4$ solutions (Figure 3) cannot be explained solely by ∼10% of inner-sphere $[Fe(SO_4)_n]^{3-2n}$ complexes. If these solutions are composed of ∼10% inner-sphere (and the rest outer-sphere complexes), then their vibrational spectra should be similar to uncomplexed sulfate/hydrogen sulfate mixture with minor changes indicating the presence of scarce inner-sphere complexes. The extensive splitting of sulfate vibrational bands and their intensities are incompatible with the conclusion drawn solely from the X-ray spectra (namely, that only ∼10% of the sulfate ions are bound in inner-sphere complexes), and the rest of sulfate occurs in outer-sphere complexes or does not associate with Fe^{III} at all. In other words, species other than outer-sphere complexes must exist in the solution, which can significantly modify the infrared spectra. They must involve strongly interacting sulfate and iron polyhedra but not through inner-sphere complex formation. Such a strong interaction between sulfate and Fe^{III} species can be facilitated by hydrogen bonds, and the hydrogen-bonded complexes are likely the abundant species responsible for the observed variation in the infrared spectra.

The tendency of sulfate and the aqueous Fe^{III} species to form hydrogen-bonded complexes is strong enough to cause conversion of hydrogen sulfate to sulfate and its binding to Fe^{III} species at pH 1. The hydrogen sulfate to sulfate conversion is documented by sharpening of the main peak in the X-ray spectra (Figure 4). It should be noted that the decline of hydrogen sulfate concentration is also caused by an increase in the ionic strength of solution (*16*). However, simultaneous increase in the intensity of bands corresponding to the hydrogen-bonded complexes, and the diminution of hydrogen sulfate spectroscopic signature indicate that the high affinity of sulfate for Fe^{III} species must be at least partially responsible for hydrogen sulfate removal from the solution.

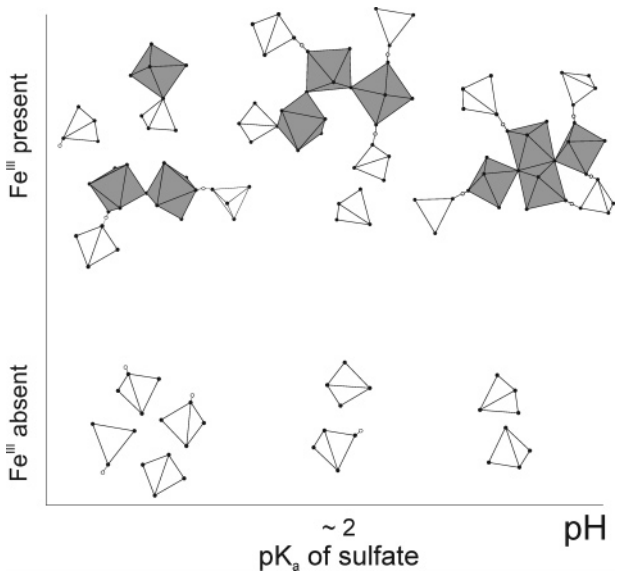

FIGURE 6. Cartoon representation of speciation in acid sulfate waters as a function of pH and Fe^{III} absence or presence. The gray polyhedra are Fe^{III} octahedra; the white ones are sulfate tetrahedra. The complexes shown are hypothetical and are depicted here to document the interaction between Fe^{III} and sulfate, either hydrogen-bonded or inner-sphere.

Results outlined in the previous paragraphs complement the speciation predictions based on interpretation of data from thermodynamic studies. The measured values for the equilibrium constant for the association reaction in aqueous phase:

$$Fe^{3+} + SO_4^{=} = [FeSO_4]^{+}$$

at 298.15 K and infinite dilution are $10^{4.27}$ (*9*) or $10^{4.04}$ (*7*). The equilibrium constants for the formation of $[Fe(SO_4)_2]^{-}$ and $[Fe(SO_4)_3]^{3-}$ have also been measured (*7*). The results of the thermodynamic studies imply that Fe^{III} and SO_4 associate strongly in the solutions, and the $[Fe(SO_4)_n]^{3-2n}$ complexes are the dominant species when sufficient sulfate is present to associate with Fe^{III}. However, they do not specify the nature of the $[Fe(SO_4)_n]^{3-2n}$ complexes. Our work shows that these $[Fe(SO_4)_n]^{3-2n}$ species are mostly hydrogen-bonded complexes, with minor proportion of inner-sphere complexes (Figure 6). Precise speciation calculations for our solutions are hampered by the lack of thermodynamic data for elevated ionic strength of Fe^{III}–SO_4 solutions.

Our study provides no information about the nature of the Fe^{III} species present in the solutions. Aqueous solutions of Fe^{III} have been investigated extensively, and polymerization has been documented by a variety of techniques (e.g., refs *10* and *23*–*25*). Magini (*23*) recognized the structural continuity between solution species and the hydrous ferric

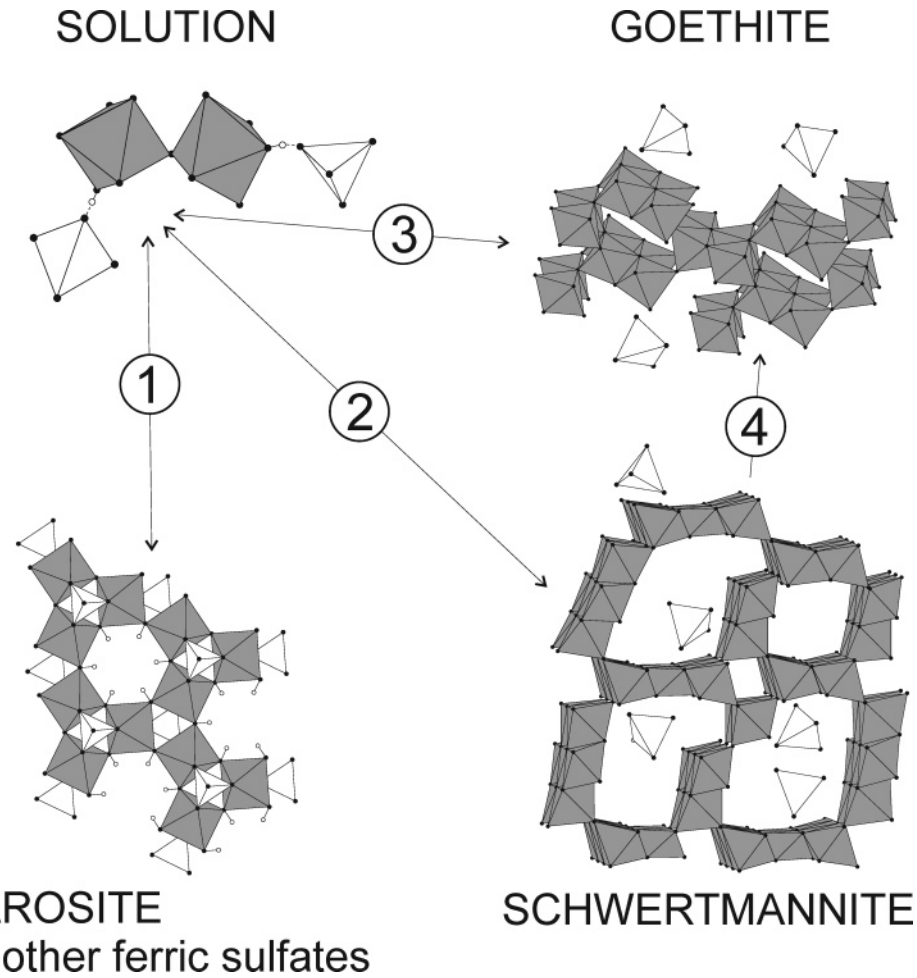

FIGURE 7. Mineral precipitation from Fe^{III}–sulfate solutions (see also Figure 3 in ref *28*). Precipitation of jarosite (reaction 1) occurs in acidic (pH < 3) solutions rich in Fe^{III}, SO_4, and K/Na and requires elevated temperature or prolonged time (*30*). Schwertmannite forms (reaction 2) from solutions with intermediate pH, and the interaction between Fe^{III}–SO_4 is identical in the solution and in the structure of this mineral. The drawing of the schwertmannite "structure" shown here is a hypothetical structure based on the results of Bigham et al. (*26*) and Waychunas et al. (*27*). At higher pH (>6), ferrihydrite or goethite with adsorbed sulfate form (reaction 3). Over time, metastable schwertmannite transforms to goethite (reaction 4) or hematite.

gels, precipitating from Fe^{III} solutions. On the basis of these studies, we assume that Fe^{III} oligomers are present in the solutions studied in this work. These Fe^{III} oligomers then interact with sulfate, mostly via hydrogen bonds, less frequently in inner-sphere complexes. Possible structures of such Fe^{III} oligomers are drawn in Figure 6. However, these structures are hypothetical, and we do not imply that these are the actual aqueous Fe^{III} oligomers in the studied solutions.

Link between Fe^{III}−SO_4 Solution Speciation and Structure of Associated Poorly Crystalline Precipitates. The Fe^{III}−SO_4 aqueous speciation, as determined in this study, is reflected in the local structure of nanocrystalline precipitates that form in acid-polluted waters. A phase encountered in acidic waters and soils is the nanocrystalline sulfate containing iron^{III} oxide schwertmannite (*26*). The structure of schwertmannite is poorly known, and its chemical composition, in terms of Fe/SO_4 and Fe/H_2O ratios, is highly variable. In schwertmannite, sulfate forms mostly H-bonded complexes in a network of disrupted, irregularly sized $Fe(O,OH,OH_2)_6$ tunnels (*26*, *27*) (Figure 7). The FTIR and XAS spectra of schwertmannite (*27*) indicate that the dominant mode of interaction between Fe^{III} and SO_4 in this phase is via hydrogen bonds. Similarly, our spectra point at the dominant occurrence of hydrogen-bonded Fe^{III}−sulfate complexes in acidic Fe^{III}−SO_4 solutions. This similarity of Fe^{III}−sulfate interaction is likely the reason why schwertmannite is commonly the initial precipitate from AMD waters. The similarity of interaction in the aqueous and solid phase may also imply that the precipitation and dissolution reaction (reaction 2 in Figure 7) is not kinetically hindered. If precipitation and dissolution is easy, then schwertmannite should be the phase that controls solubility and speciation of Fe^{III}, SO_4, and indirectly also other components in the solution.

Acid mine waters precipitate a plethora of minerals, not only schwertmannite. At low pH, jarosite may occur; at circumneutral pH, ferrihydrite and goethite form (*28*, *29*) (Figure 7). Formation of the well-crystalline ferric sulfate minerals may require prolonged time; elevated temperatures; high concentration of Fe^{III}, SO_4, and H^+; or the presence of additional ions, such as Na and K for jarosite (*30*). In jarosite and other ferric sulfate minerals, sulfate tetrahedra and iron octahedra are always linked by at least one bridging oxygen (*31*), in contrast with dominant hydrogen-bonding interaction in our solutions. It is possible that the aqueous speciation in very acidic or concentrated AMD solutions is different from what was observed in the solutions studied in this work. At mildly acidic to circumneutral pH, ferrihydrite or goethite precipitate and sorb sulfate on their surfaces (Figure 7). At the surface of goethite, sulfate ions form a mixture of inner-sphere, hydrogen-bonded, and outer-sphere complexes (*17*, *20*).

We speculate that comparable links exist in other aqueous systems that precipitate poorly crystalline or X-ray amorphous solids. Similar questions may be brought up, similar answers sought, and similar links found in many other aqueous systems, not just acidic or polluted waters. A better understanding of aqueous speciation would shine light on relationships between solution complexes and solids, solubility, and bioavailability of metals.

Acknowledgments

We thank A. Leri (Princeton University) for collecting some of the sulfur X-ray spectra used in this study; J. E. Post (Smithsonian Institution) and C. N. Alpers (USGS) for providing iron sulfate standards used in this investigation; and C. Cravotta (USGS) for useful discussion of the AMD systems. We also appreciate the help of beamline scientists and researchers at the Stanford Synchrotron Radiation Laboratory (B. Hedman, G. N. George) and National Synchrotron Light Source (W. Caliebe). This research was supported by the Hess Post-doctoral Fellowship (Department of Geosciences, Princeton University) and the NSF (CRAEMS).

Literature Cited

(1) Stoddard, J. L.; Jeffries, D. S.; Lukewille, A.; Clair, T. A.; Dillon, P. J.; Driscoll, C. T.; Forsius, M.; Johannessen, M.; Kahl, J. S.; Kellogg, J. H.; Kemp, A.; Mannio, J.; Monteith, D. T.; Murdoch, P. S.; Patrick, S.; Rebsdorf, A.; Skjelkvale, B. L.; Stainton, M. P.; Traaen, T.; van Dam, H.; Webster, K. E.; Wieting, J.; Wilander, A. Regional trends in aquatic recovery from acidification in North America and Europe. *Nature* **1999**, *401*, 575−578.

(2) Carmichael, G. R.; Streets, D. G.; Calori, G.; Amann, M.; Jacobson, M. Z.; Hansen, J.; Ueda, H. Changing trends in sulfur emissions in Asia: Implications for acid deposition, air pollution, and climate. *Environ. Sci. Technol.* **2002**, *36*, 4707−4713.

(3) Nordstrom, D. K.; Alpers, C. N.; Ptacek, C. J.; Blowes, D. W. Negative pH and extremely acidic mine waters from Iron Mountain, California. *Environ. Sci. Technol.* **2000**, *34*, 254−258.

(4) Buckby, T.; Black, S.; Coleman, M. L.; Hodson, M. E. Fe-sulphate-rich evaporative mineral precipitates from the Rio Tinto, southwest Spain. *Mineral. Mag.* **2003**, *67*, 263−278.

(5) Parkhurst, D. L.; Thorstenson, D. C.; Plummer, L. N. A computer program for geochemical calculations. *Water Resour. Invest.* (*U.S. Geol. Surv.*) **1980**, *No. 80-96*, 195 pp (revised and reprinted, 1990).

(6) Bigham, J. M.; Nordstrom, D. K. Iron and aluminum hydroxysulfates from acid sulfate waters. In *Sulfate Minerals*: *Crystallography, Geochemistry and Environmental Significance*; Alpers, C. N.; Jambor, J. L.; Nordstrom, D. K., Eds.; Reviews in Mineralogy and Geochemistry 40; Mineralogical Society of America: Washington, DC, 2000; pp 351−404.

(7) Mattoo, B. N. Stability of metal complexes in solution. III. Ion association in ferric sulphate and nitrate solutions at low Fe III concentration. *Z. Phys. Chem. Neue Folge* **1959**, *19*, 156−167.

(8) Sapieszko, R. S.; Patel, R. C.; Matijevic, E. Ferric hydrous oxide sols. 2. Thermodynamics of aqueous hydroxo and sulfato ferric complexes. *J. Phys. Chem.* **1977**, *81*, 1061−1068.

(9) Millero, F. J.; Yao, W.; Aicher, J. The speciation of Fe(II) and Fe(III) in natural waters. *Mar. Chem.* **1995**, *50*, 21−39.

(10) Shaw, S.; Warner, J. A.; Benning, L. G.; Brown, G. E. Jr. SAXS/WAXS studies of the precipitation and crystallisation of iron and aluminium (oxy)hydroxides. *Geochim. Cosmochim. Acta* **2002**, *66*, A704.

(11) Lyon, J. S.; Hilliard, T. J.; Bethell, T. H. *Burden of Guilt*; Mineral Policy Center: Washington, DC, 1993.

(12) Ressler, T. WinXAS: a program for X-ray absorption spectroscopy data analysis under MS-Windows. *J. Synchrotron Radiat.* **1998**, *5*, 118−122.

(13) Jiang, D. T. X-ray absorption fine structure spectroscopy. In *Synchrotron Radiation. Earth, Environmental and Materials Science Applications*; Henderson, G., Baker, D. R., Eds.; Mineralogical Association of Canada Short Course Series 30; Mineralogical Association of Canada: 2002; pp 65−98.

(14) Larson, A. C.; von Dreele, R. B. *GSAS. General Structure Analysis System.* LANSCE, MS-H805: Los Alamos, NM, 1994.

(15) Hug, S. J. In situ Fourier transform infrared measurements of sulfate adsorption on hematite in aqueous solutions. *J. Colloid Interface Sci.* **1997**, *188*, 415−422.

(16) Dickson, A. G.; Wesolowski, D. J.; Palmer, D. A.; Mesmer, R. E. Dissociation constant of bisulfate ion in aqueous sodium chloride solutions to 250 °C. *J. Phys. Chem.* **1990**, *94*, 7978−7985.

(17) Peak, D.; Ford, R. G.; Sparks, D. L. An in situ ATR-FTIR investigation of sulfate bonding mechanisms on goethite. *J. Colloid Interface Sci.* **1999**, *218*, 289−299.

(18) Myneni, S. C. B. X-ray and vibrational spectroscopy of sulfate in Earth materials. In *Sulfate Minerals*: *Crystallography, Geochemistry, and Environmental Significance*; Alpers, C. N., Jambor, J. L., Nordstrom, D. K., Eds.; Reviews in Mineralogy and Geochemistry 40; Mineralogical Society of America: Washington, DC, 2000; pp 113−172.

(19) Okude, N.; Nagoshi, M.; Noro, H.; Baba, Y.; Ymamoto, H.; Sasaki, T. A. P and S K-edge XANES of transition-metal phosphates and sulfates. *J. Electron Spectrosc. Relat. Phenom.* **1999**, *101−103*, 607−610.

(20) Myneni, S. C. B.; Waychunas, G. A.; Traina, S. J.; Brown, G. E., Jr. Understanding the speciation of oxoanions in aquatic systems. *Science* (submitted for publication).

(21) Xiao, C.; Wesolowski, D. J.; Palmer, D. A. Formation quotients of aluminum sulfate compexes in $NaCF_3SO_3$ media at 10, 25,

and 50 °C from potentiometric titrations using a mercury/mercurous sulfate electrode concentration cell. *Environ. Sci. Technol.* **2002**, *36*, 166−173.
(22) Reardon, E. J.; Beckie, R. D. Modeling chemical-equilibria of acid mine-drainage—The $FeSO_4$−H_2SO_4−H_2O system. *Geochim. Cosmochim. Acta* **1987**, *51*, 2355−2368.
(23) Magini, M. Structural relationships between colloidal solutions and hydroxide gels of iron(III) nitrate. *J. Inorg. Nucl. Chem.* **1977**, *39*, 409−412.
(24) Combes, J. M.; Manceau, A.; Calas, G.; Bottero, J. Y. Formation of ferric oxides from aqueous-solutions—A polyhedral approach by X-ray absorption-spectroscopy. 1. Hydrolysis and formation of ferric gels. *Geochim. Cosmochim. Acta* **1989**, *53*, 583−594.
(25) Näslund, L.-A.; Cavalleri, M.; Ogasawara, H.; Nilsson, A.; Pettersson, L. G. M.; Wernet, P.; Edwards, D. C.; Sandström, M.; Myneni, S. Direct evidence of orbital mixing between water and solvated transition-metal ions: An oxygen 1s XAS and DFT study of aqueous systems. *J. Phys. Chem.* **2003**, *A107*, 6869−6876.
(26) Bigham, J. M.; Schwertmann, U.; Carlson, L.; Murad, E. A poorly crystallized oxyhydroxysulfate of iron formed by bacterial oxidation of Fe(II) in acid-mine waters. *Geochim. Cosmochim. Acta* **1990**, *54*, 2743−2758.
(27) Waychunas, G. A.; Myneni, S. C. B.; Traina, S. J.; Bigham, J. M.; Fuller, C. C.; Davis, J. A. Reanalysis of the schwertmannite structure and the incroportation of SO_4^{2-} groups: An IR, XAS, WAXS and simulation study. *Abstracts of the 11th Goldschmidt Conference*; 2001.
(28) Bigham, J. M.; Schwertmann, U.; Carlson, L. Mineralogy of precipitates formed by the biogeochemical oxidation of Fe(II) in mine drainage. In *Biomineralization Processes of Iron and Manganese*: *Modern and Ancient Environments*; Skinner, H. G. W., Fitzpatrick, R. W., Eds.; Catena Supplement 21; Catena-Verlag: Cremlingen-Destedt, Germany, 1992; pp 219−232.
(29) Schwertmann, U.; Bigham, J. M.; Murad, E. The 1st occurrence of schwertmannite in a natural stream environment. *Eur. J. Mineral.* **1995**, *7*, 547−552.
(30) Bigham, J. M. Personal communication.
(31) Hawthorne, F. C.; Krivovichev, S. V.; Burns, P. C. The crystal chemistry of sulfate minerals. In *Sulfate Minerals*: *Crystallography, geochemistry, and environmental significance*; Alpers, C. N., Jambor, J. L., Nordstrom, D. K., Eds.; Reviews in Mineralogy and Geochemistry 40; Mineralogical Society of America: Washington, DC, 2000; pp 1−112.

Received for review March 3, 2004. Revised manuscript received September 30, 2004. Accepted October 4, 2004.

ES049664P